Lab on a Chip

Non-contact monitoring of extra-cellular field potentials with a multi-electrode array

Journal:	*Lab on a Chip*
Manuscript ID	LC-ART-09-2018-000984.R2
Article Type:	Paper
Date Submitted by the Author:	22-Jan-2019
Complete List of Authors:	Sharf, Tal; University of California Santa Barbara, Neuroscience Research Institute; Hansma, Paul; University of California Santa Barbara, Department of Physics Hari, Mukund; University of California Santa Barbara, Department of Molecular, Cellular and Developmental Biology Kosik, Kenneth; University of California Santa Barbara, Neuroscience Research Institute

SCHOLARONE™
Manuscripts

Non-contact monitoring of extra-cellular field potentials with a multi-electrode array

Tal Sharf,[†, ‡] Paul K. Hansma, [£,†] Mukund A. Hari[‡] and Kenneth S. Kosik[†,‡]

[†] Neuroscience Research Institute, University of California Santa Barbara, Santa Barbara, CA 93106

[‡] Department of Molecular, Cellular and Developmental Biology, University of California Santa Barbara, Santa Barbara, CA 93106

[£] Department of Physics, University of California Santa Barbara, Santa Barbara, CA 93106

Correspondence and requests for materials should be addressed to T.S. (email: talsharf@ucsb.edu)

ABSTRACT: Developing tools to enable non-invasive, high-throughput electrophysiology measurements of large functional-networks of electrogenic cells used as *in vitro* disease models for the heart and brain remains an outstanding challenge for preclinical drug discovery, where failures are costly and can prove to be fatal during clinical trials. Here we demonstrate, for the first time, that it is possible to perform non-contact monitoring of extra-cellular field potentials with a multi-electrode array (MEA). To do this preliminary demonstration we built a

prototype with a custom mechanical stage to micro-position cells grown on

conventional glass coverslips over the recording surface of a MEA sensor. The

prototype can monitor extra-cellular fields generated by multi-cellular networks in a

non-contact configuration, enabling a single MEA sensor to probe different cultures

in succession, without fouling or degrading its sensitive electronic surface. This first

demonstration with easy to culture cardiomyocyte cells and a prototype device

points to the exciting possibility for instrument development leading to more efficient

and cost-effective drug screening paradigms for cardiovascular and neurological

diseases.

Introduction

Recent breakthroughs in cell-culturing techniques used to model functional

human organs, known as organ-on-chips, offer the potential to revolutionize methods for

drug discovery and efficacy. A major focus is geared toward the subset of electrogenic

cells found in the heart and brain.[1–4] State-of-the-art advances in neurobiology range

from the generation of a multitude of specific neuronal subtypes,[5,6] to bioengineering

reproducible cortical tissue architecture[7] and assembling a functionally integrated

human forebrain.[8] Meanwhile, cutting-edge developments in cardiology have led to the

recreation of key elements of the heart,[9] which include pacemaker cells[10] and the

development of cardiac tissue displaying adult-like gene profiles,[11] all grown from

human pluripotent stem cells. The ability to observe electrical activity of large multi-

cellular populations with single-cell resolution is a crucial step towards uncovering basic

principles that govern their function, which may transform our understanding of and

approach to treating disease.[12–15]

These advances are made more exciting in light of breakthroughs in monitoring

the electrical activity of cells using high resolution multi-electrode arrays (MEAs).

Recently, Tsai *et al.*[16] demonstrated the capacity to record simultaneously from 17,000

neurons across an entire retina using complementary metal-oxide-semiconductor

(CMOS) electronics. The rapidly advancing field of MEA technology,[17,18] which include

integration of nano-structured recording electrode techniques developed by Abbot *et*

al.[19] with CMOS, is enabling the study of large cell populations with unprecedented

spatiotemporal resolution.

One problem in using these breakthroughs to enhance our understanding of

human neurodegenerative and cardiovascular disease is that it is not possible to do

high-throughput experiments because of the cost and difficulty of culturing cells on

multi-electrode arrays (MEAs). Firstly, specialized micro-patterning techniques are

required to generate functional surfaces with the capacity to template spatial cellular

organization. This is commonly achieved by modifying the chemical structure,[20,21] or by

bonding of a microfluidic device to the MEA surface.[22–24] The complexity of these bio-

electronic interfaces makes them inherently difficult to reuse; cellular debris can foul

their sensitive surfaces. Furthermore, chemical and plasma-based cleaning methods,

common within the microfabrication community, are not readily accessible to the

biological research community. As a result, probing the electrical activity of electrogenic

cells grown directly on custom-microelectronics remains a costly and labor-intensive

process, one difficult to scale for high-throughput drug screening assays.

Here we report, for the first time, a method that can apply the power of multi-electrode arrays (MEAs) to cells grown on conventional glass coverslips, providing a new platform to conduct high-throughput electrophysiology measurements at the network level using a single MEA sensor (Figure 1). For this first report we chose cardiomyocytes because they are more robust and easy to grow for a proof of principle. Clearly this is just a first step on a path that could lead to a practical instrument that could also perform measurements on neurons.

Culturing cells on glass coverslips is a standard practice in the biological sciences and these substrates are easily micro-patterned to template spatial cellular organization[25–28] and tune mechanical interactions with their environment.[29,30] First, we implement a mechanically adjustable stage, based on techniques used to create squeezable electron-tunneling junctions,[31,32] to lower cultures of hundreds of networked cardiomyocytes towards the sensing surface of a MEA and observe their network activity. Our attempts to use this prototype on neurons were unsuccessful. We believe this was due to shear forces when removing the cells from growth medium and placing

them into liquid reservoir of the MEA with the mechanical stage (see Results and

Discussion for details on how the cells are interfaced with the MEA). Our lab, as well as

others have demonstrated that it is possible to detect extra-cellular fields from neurons

grown in culture wells using a single, mobile micro-electrode in a non-contact

configuration.[33,34] These observations point to the need for an instrument that lowers the

MEA to the cells, which can be left undisturbed in their culture wells. This instrument is

under development in our lab.

The general principle is to mechanically move and hold a MEA, close enough to

the cells to do electrophysiology recordings as shown in Figure 1. Either the MEA can

be moved to the cells or the cells can be moved to the MEA. If the MEA is moved, the

cells can remain undisturbed, which is a major advantage. For this initial demonstration

we moved the cells so that we could use our commercial MEA without modification. For

cardiomyocytes we observed propagating signals with signal-to-noise ratios comparable

to cardiomyocytes grown directly on the recording surface of the MEAs (See supporting

Info Section A and B for representative extra-cellular field potential wave forms).[35,36]

Additionally, the mechanical stage operates without any observable drift or hysteresis

and does not require active feedback controllers to maintain its position. This new

technique will enable low-cost, high-throughput measurements of networked cellular

activity and aid in the development of therapies intended to treat heart and brain

disease.[13,37–39]
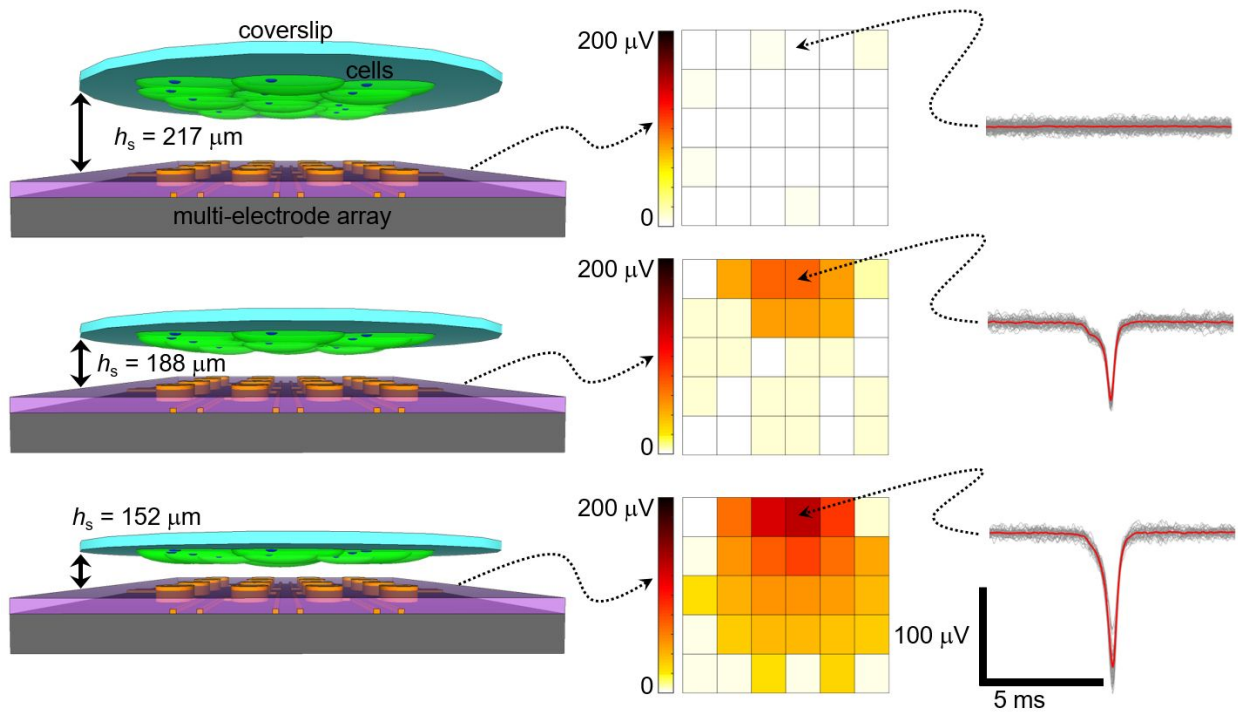
Figure 1. Non-contact measurements of extra-cellular field potentials were performed by lowering electrogenic cells towards the surface of a multi-electrode array (MEA). A custom mechanically actuated stage is used to control the relative distance between the cells and the recording surface of the MEA. Extra-cellular field potentials are shown as a function of time for a spatial cluster of cellular activity produced by a cardiomyocyte culture at 20 days *in vitro*. For visual clarity, spike-detected voltage amplitudes are displayed in a 6 by 6 grid (from adjacent electrodes) to highlight a region of cellular activity as the coverslip approaches the MEA surface. The extra-cellular voltage vs. time recorded by a single electrode (dotted arrow) during approach is shown on the right side. Individual spikes, center about their spike time, are plotted in gray, while the spike triggered average is shown in red. Each electrode is 30 μm in diameter spaced at 100 μm pitch. As the cells approach the recording surface, the signals can be easily detected above background noise fluctuations. This method can be used to successively monitor different cell cultures using the same MEA.

Results and Discussion

Device design and characterization. To bring the power of multi-electrode arrays

(MEAs) to cells grown on coverslips, we have developed a novel approach involving

lowering the coverslip onto a MEA using magnetic force (Figure 2). This approach has

the advantage that it does not rely on cell cultures to be grown on the surface of

sensitive electronics. Rather, cell cultures can be grown on cheap and disposable

commercial glass coverslips and then gently micro-positioned above a recording

electrode surface using the mechanical stage. The surface height, h_s, of a glass

coverslip can be tuned by varying the distance, d_m, between a large magnet and a small

magnet. The resultant force applied to the small magnet, due to magnetic-dipole

repulsion, can be tuned over a continuous range by controlling the separation distance

between the two magnets d_m. There is a demagnification factor of approximately 140

between the distance d_m, which is mechanically controlled (Figure 2a) and h_s, which is

the distance between the cells and the recording surface (Figure 2c,d,e). This

mechanical positioning technique was inspired by methods used to create electron

tunnel junctions, which can attain sub-nanometer positioning precision.[31,32] Moreover,

the properties of the simple mechanical stage allow for hysteresis free operation when

cycling through its dynamic range, giving the precision of piezoelectric stage without the

use of complex feedback controllers necessary to maintain their position. For further

details about the mechanical reproducibility and angular variability of the coverslip

during approach see Supporting Info Section C.
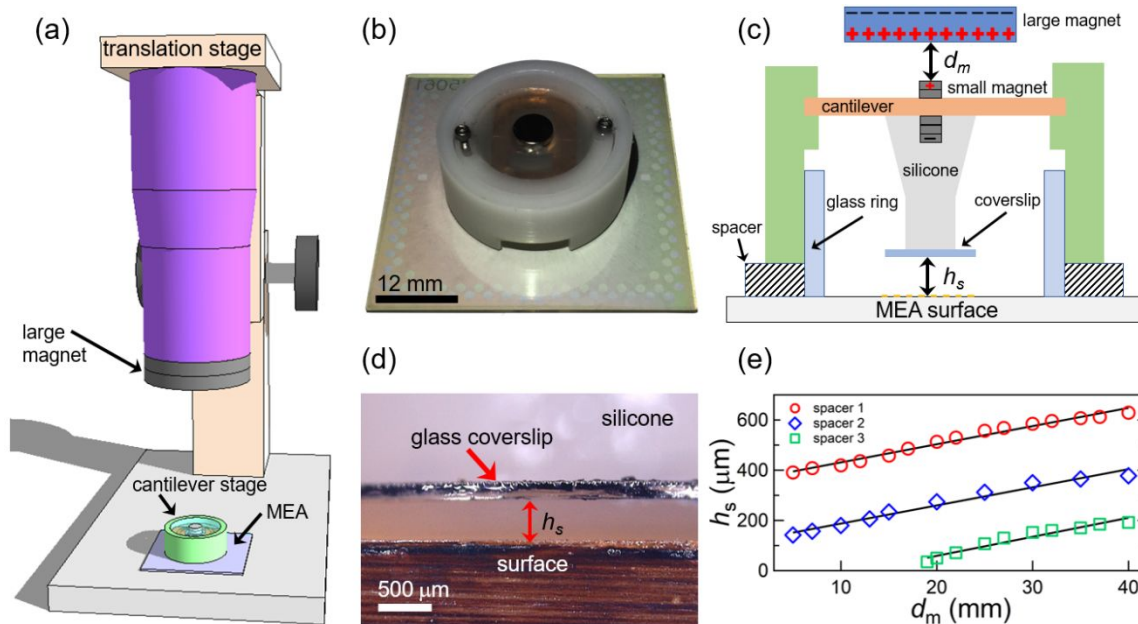
Figure 2. Overview of the mechanical stage used to micro-position a glass coverslip containing a culture of electrogenic cells above the surface of a multi-electrode array (MEA). (a) Schematic overview of the magnetically actuated positioning stage. A small cantilever is used to vertically micro-position an electrogenic cell culture above the recording surface of a MEA. The force exerted on the cantilever (due to magnetic dipole-dipole repulsion) can be tuned over a continuous range by varying the separation distance between the two magnets. (b) Photograph of the positioning stage mounted on top of a MEA. The scale bar is 12 mm. (c) Cross sectional diagram of micro-positioning stage positioned above the recording surface of a MEA. (d) Optical image of a glass coverslip positioned above a glass surface. The scale bar is 500 μm. (e) Measured coverslip height above the surface h_s as a function of large-magnet to small-magnet separation distance d_m. The cantilever deflection is 7.2 ± 0.3 μm for every mm change in d_m. Three different vertical indexing spacers (diagramed in c) were used to offset the dynamic range (240 μm) of the stage.

Non-contact measurements of extra-cellular field potentials. To demonstrate the principle of using a multi-electrode array (MEA) as a non-contact, multi-cellular electrophysiology probe, we first prepared primary cardiomyocyte cultures on glass coverslips using conventional techniques (see Methods and Supporting Info Section D for microscopy and characterization of cell morphology). A coverslip containing cells in culture was then mounted onto the micro-positioning stage and lowered towards the surface of the MEA to record their electrical activity. The amplitude of extra-cellular fields measured by the MEA increases as the relative distance to the cells decreases. These fields are observable when their measured amplitude exceeds background electronic noise fluctuations sensed by the recording electrodes.

Figure 3 highlights the dramatic difference between using an MEA in the non-contact configuration versus the traditional contact-configuration, where cells are grown directly on the sensor surface. In the non-contact configuration (Figure 3a), the MEA remained like new after probing $N = 10$ separate cell cultures. Meanwhile an MEA used in the traditional contact-configuration (Figure 3b) after $N = 8$ cultures can no longer can

detect extra cellular field potentials. This is largely due to a continual build of cellular

debris and electrode degradation as a result of replating cells directly onto the same
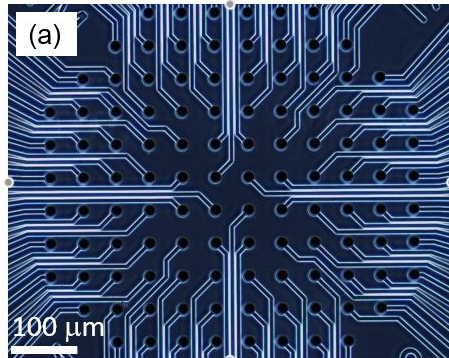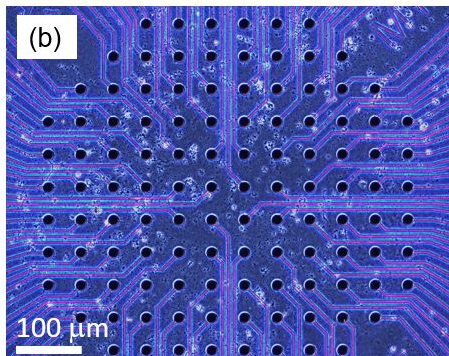
surface.

Figure 3. (a) Phase contrast images of a multi-electrode array (MEA) used in the non-contact configuration for N = 10 different cell culture preparations. (b) Cells were grown on a MEA surface in the traditional contact-configuration. The scale bar is 100 μm.

Figure 4 shows spontaneous spiking activity produced by a medium-density

culture (17 days *in vitro*) positioned at a fixed height (h_s = 391 μm) above the recording

surface of a MEA. The upper three arrows highlight observable extra-cellular field potentials produced by the 'beating' of cells that form a contiguous cluster that spans across much of the array. The spatial extent of the observed activity is indicated by the blue squares. Regions outside of the cell clusters are electrically inactive and register only electronic noise, as shown by the lower left arrow of Figure 4. Extra-cellular field potentials were recorded from low-density single cell preparations to confluent cardiomyocyte sheets ranging from 4 to 21 days *in vitro* (DIV) from a total of $N = 10$ different cell culture preparations (see Methods). To characterize the spatial dependence of extra-cellular field potentials, we focus on low-density, single cell clusters plated at a density of $125{,}000$ cells·cm^{-2} before 7 DIV and medium-density cultures that have proliferated into large, multi-cellular clusters at later time points consisting of a confluent network of cells that span several hundreds of microns in diameter.
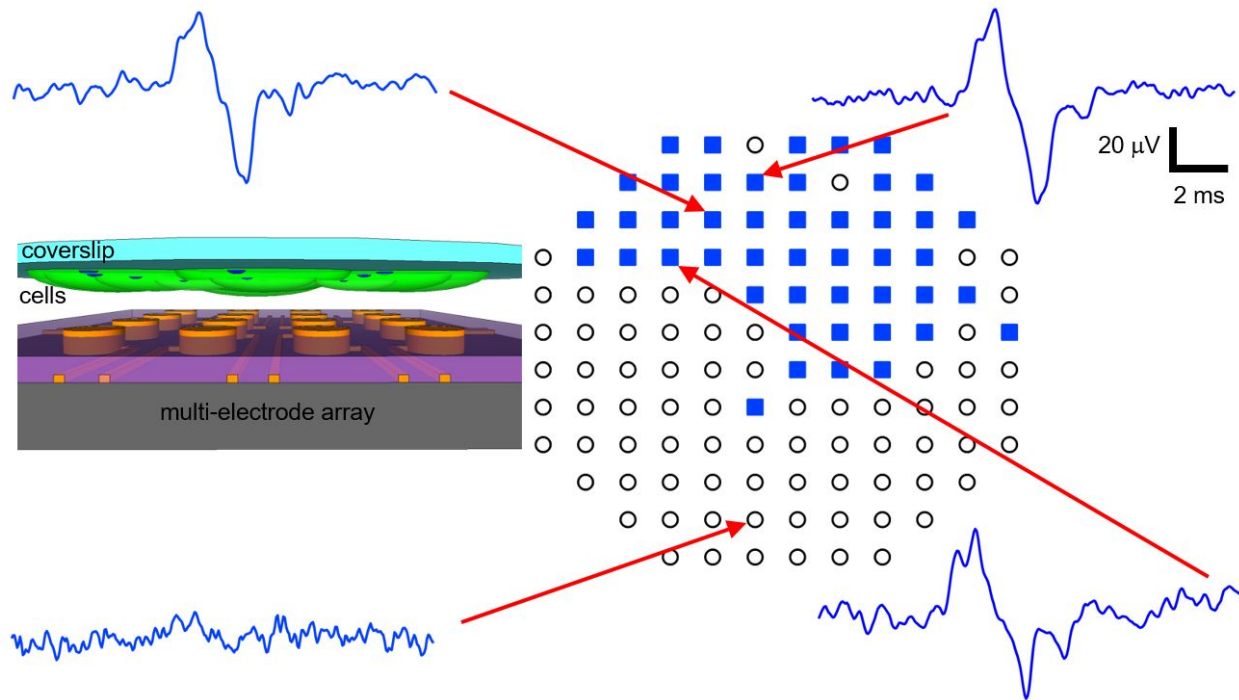
Figure 4. Measured voltage of extra-cellular field potentials generated by a culture of cardiomyocytes (17 days *in vitro*) positioned above the surface of a multi-electrode array (MEA) at a fixed height of 391 μm. The vertical and horizontal scale bars are 20 μV and 2 ms, respectively. Red arrows specify the spatial locations as measured by the MEA. The blue squares indicate electrode locations that detected extra-cellular field potentials produced by cells residing above their surface, while the open circles are spatial regions where no signals were detected above background noise fluctuations. The MEA consists of 120 recording electrodes, each with a 30 μm diameter, spaced at a 100 μm pitch. The cartoon diagram on the left depicts the experimental setup with a coverslip containing cells positioned above the recording electrodes.

Distance dependence of extra-cellular field potentials. To demonstrate the reliable

spatial control of the height, we first show that the magnitude of the extra-cellular field

potentials can be modulated by varying the relative distance of the cell culture from the

recording surface of the MEA. Figure 5a shows experimentally measured voltage as a

function of time as a cardiomyocyte culture (6 DIV) approaches and leaves the MEA

surface over a continuous range of surface heights h_s. No signals are detected (above

background noise fluctuations) in the resting position of h_s = 590 μm. As the stage is

lowered, h_s is decreased and extra-cellular field potentials become detectable at $h_s \sim$

234 μm (figure 5b). The voltage amplitude increases significantly for h_s < 234 μm.

Repeated cycling of the stage does not vary the voltage amplitude (within experimental

uncertainty) for fixed values of h_s.
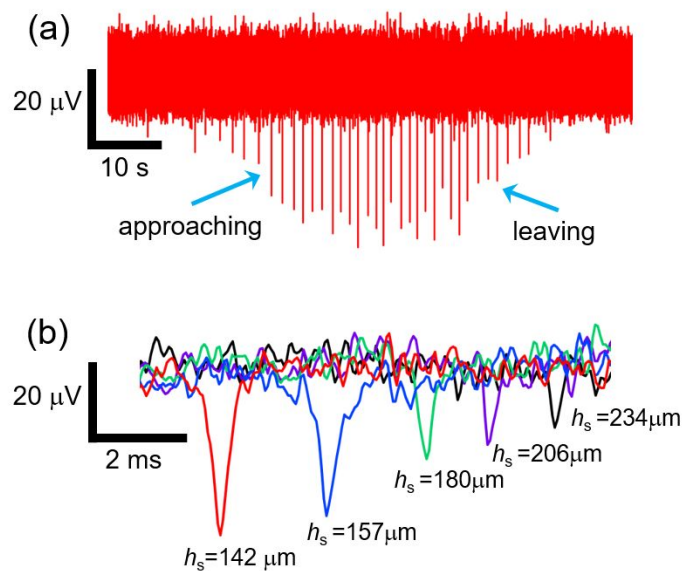
Figure 5. Distance dependence of extra-cellular field potentials (a) Measured extra-cellular voltage vs. time as a cardiomyocyte culture (low density, clusters of single cells,

6 days *in vitro*) approaches and leaves the recording surface of a MEA. Vertical and horizontal scale bars are 20 μV and 10 s, respectively. (b) Individual extracellular voltage vs. time traces for fixed surface heights h_s above the MEA surface. The traces are offset horizontally for clarity. Vertical and horizontal scale bars are 20 μV and 2 ms, respectively.

We first note that the origin of the extra-cellular field potentials produced by electrogenic cells are generated by the flow of transmembrane ionic currents.[40–42] However, the magnitude of these fields depends critically on the ion channel density distributed across the cell membrane, which increases with cell maturation.[43] Additionally, spatiotemporally synchronized cellular activity mediated via gap-junctions,[44] generates a net additive effect on the magnitude of extra- cellular filed potentials, a result due to the linear superposition principle.[41,45] In short, un-synchronized young populations of cells generate smaller extra-cellular fields compared to more mature and synchronized populations.[46] Additionally, extra-cellular waveforms generated by cardiomyocytes can vary dramatically depending on various components of the transmembrane ion current and capacitive components as shown by Tertoolen *et*

al.[47] with their richly detailed calculation and simulations. See Supporting Info Section E

for details about modeling the magnitude of transmembrane ionic currents as a function

of distance from the cell's surface using a simple volume conduction model. Further

experiments and instrumentation development would be needed to simultaneously

visualize and monitor the extra-cellular field potentials in the non-contact configuration

during approach to thoroughly investigate the effects of cell maturation and

synchronization on the magnitude of the extra-cellular field potentials.

Shape and distribution of extra-cellular field potentials. Simultaneous measurements

performed on MEAs using patch-clamp have previously demonstrated that extra-cellular

field potentials accurately reflect the local changes in the membrane potential of

cardiomyocytes.[35,48,49] However, outward currents generated by simultaneous

depolarization from neighboring cells, as well as passive capacitive currents, will

generate initial positive components to the extra-cellular waveform. These effects

generate regional differences in waveforms that depend on the relative distance of the

recording electrode to the local distribution of active and passive current sources, which

form the resultant extra-cellular field potential.[35,50] Extra-cellular fields are further

modulated by the resistance and capacitance of the recording electrodes, but can still

be used to accurately reconstruct the action potential waveforms

observed by patch clamp measurements.[47] These combined effects account for the

spatial waveform variation across the MEA (for example see Figure 6) as well as

distance related effects as shown in Supporting Info Section E Figure S5. We observe

similar waveform distributions for measurements made in the non-contact configuration

(see Supporting Info Section A) compared to control measurements in the conventional

contact configuration, where cells are grown on the surface of the MEA (see Supporting

Info Section B).

Resolving spatiotemporal activity. Generating high-resolution maps of impulse

propagation along cardiac tissue is crucial for developing *in vitro* models as a test bed

for regenerative tissue research.[51,52] We demonstrate that the positioning stage can be

used to probe spatiotemporal activity of cardiomyocyte cultures grown on coverslips

using the MEAs in a non-contact configuration. Figure 6a shows a temporal activation

map of an electrical impulse propagating across a cardiomyocyte culture (17 DIV)

positioned above the surface of a MEA. The impulse is first observed by the electrode

indicated by the 'x' and propagating outwards. Representative voltage traces are shown

by Figure 6b, which indicate the temporal latencies between the spikes at different

positions measured along the MEA (shown by the dotted lines). From this activation

map we observe an average propagation velocity of v_p = 0.27 ± 0.11 m·s^{-1}, which is

bounded by previous observations, which span from 0.13 m·s^{-1} to 0.36 m·s^{-1} depending

on cell orientation.[44,46,53]
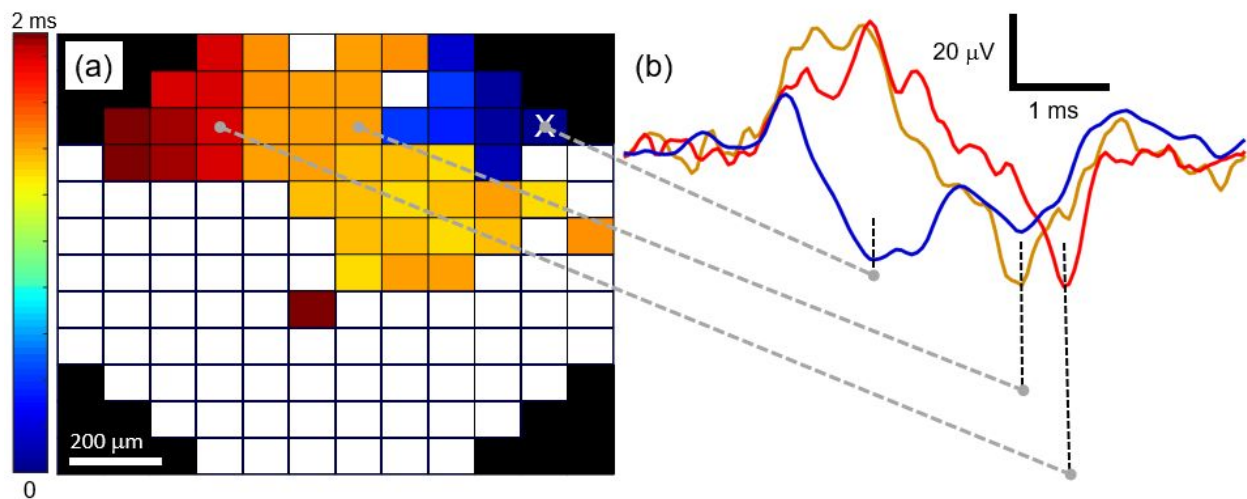
Figure 6. (a) Spatiotemporal activation map of action potentials generated within a
cardiomyocyte culture (17 days *in vitro*) positioned above the recording surface of a

MEA. The activation origin is denoted by the 'x'. (b) Extra-cellular voltage signals measured by the MEA highlight the spatiotemporal activation delays. Vertical and horizontal scale bars are 20 μV and 1 ms, respectively. The dotted lines indicate the spatial location of the recording. The different shapes of the action potentials shown here are similar to the different shapes in contact recordings. They are due to differing relative contributions of capacitive and resistive components of the ionic current as explained above in the section on shape and distribution of extra-cellular field potentials.

We next demonstrate that this technique can be utilized to resolve sub-cellular activity with high temporal resolution. For this purpose, we utilize low-density cell culture preparations consisting primarily of single cells measured before 7 DIV. Figure 7 shows an activation map of two independently temporally correlated regions of activity. The source of activity is initiated spatially at locations designated by the 'x' and propagate outwards. The short temporal delays are indicative of intercellular signal propagation caused by the cascading wave of ion channel activation associated with action potential propagation signals.[54] The negative peaks are the result of active transmembrane current flow, while the positive peaks are the result of passive capacitive currents.[35,55] The spatial distribution of these fields are reasonable, given single cardiomyocytes can reach lengths of up to ~150μm[56,57] (see Supporting Info Section D for microscopy of cell cultures) and their extra-cellular fields can be detected at distances of greater than 50

μm from the cell body,[35] a result consistent with our low-density measurements (Figure

5b).
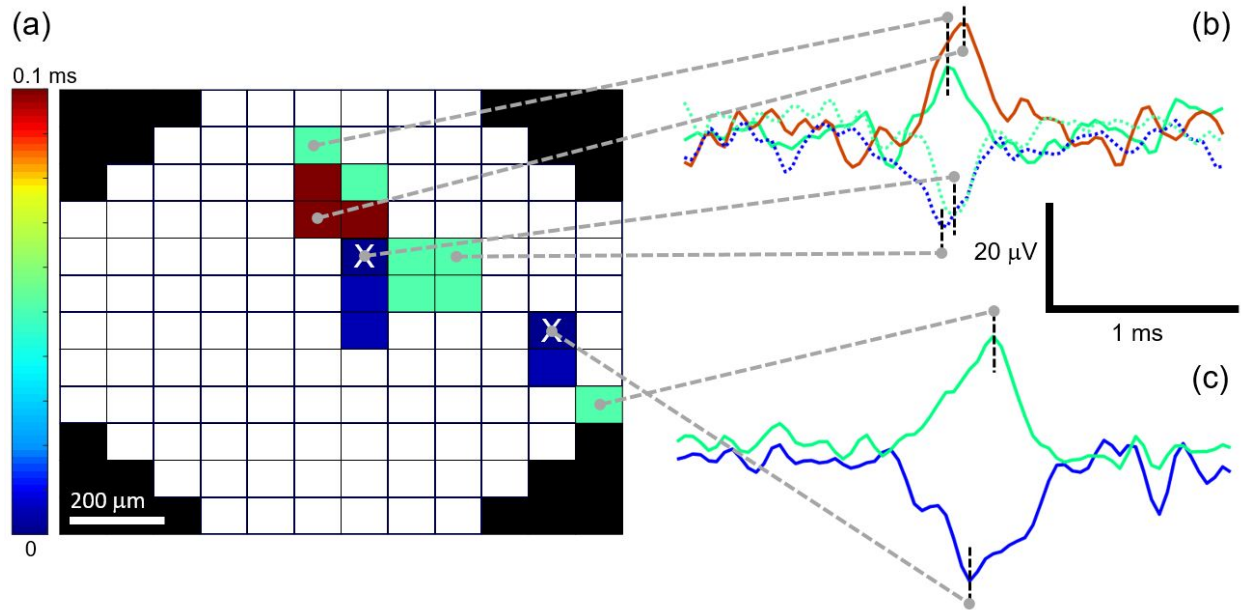
Figure 7. (a) Spatiotemporal activation map of action potentials of isolated, low density, 'single' cell populations of cardiomyocytes (6 DIV) positioned above the recording surface of a MEA. (b-c) Two spatially distinct 'single' cell clusters are highlighted by the extracellular voltage signals measured by the MEA. The 'x' marks the temporal activation origin for each cell cluster. Vertical and horizontal scale bars are 20 μV and 1 ms, respectively.

Conclusion

Our measurements demonstrate the exciting possibility for development of faster

and cheaper methods to investigate multi-cellular scale electrical signaling and pave a

route towards the developing high-throughput pharmacological screens intended to

understand and treat disease. Further research is urgently needed to move from the

prototype demonstration device to a practical instrument. In particular, it would be better

to lower the MEA down to the cells rather than lower the cells to the instrument because

then we could do measurements on cultured cells in conventional multi-well plates.

Methods

Positioning stage design. The micro-positioning stage was designed using the 3D
modeling software SketchUp (Trimble Inc.)

Mechanical stage fabrication. The mechanical stage is composed of five components:

(1) Cantilever support housing, (2) magnetic cantilever, (3) silicone coverslip mounting

column, (4) magnetic translation stage, and (5) height indexing spacers. (1) The

cylindrical support for the cantilever was machined out of Delrin (McMaster-Carr) stock

material (1.25" diameter rod) and designed to fit snuggly around the glass ring attached

to the MEA (0.945" OD). (2) The central cantilever was cut out of 0.005" thick 510

bronze sheets (McMaster-Carr) and sandwiched between a vertical stack of 0.25"x 0.1"

neodymium magnets (McMaster-Carr) with 1.8 lbs. max pull; two magnets attach above

the center of the cantilever and three below (cantilever-stack). (3) The central column,

used to mount coverslips, was cast out of two-part silicone (ecoflex 0030, Reynolds

Advanced Materials) and encapsulated the magnetic cantilever. A machined Delrin

mold insert was used for the casting. The silicone was cured at room temperature for 12

hours before releasing the mold. (4) A vertical translation stage from a stereoscopic

microscope (Edmond Scientific) was modified to mount two stacked 2"x1/4" neodymium

magnets (stage-stack) with a 35 lbs. max pull (McMaster-Carr). The two magnetic

stacks (stage and cantilever) were oriented so the dipoles repelled one another. The

vertical translation stage was used to vary the vertical separation between the stage-

stack relative to the cantilever-stack, thus applying a variable force to the cantilever. (5)

The resting height of a coverslip mounted to the silicone column was vertically offset

using indexing spacers made of sandwiched glass coverslips with a thickness of ≈ 160

μm.

Positioning stage calibration. A digital 200x microscope (5 MP, Celestron) was used to

image the surface separation height h_s of the coverslip (≈ 160 μm thick) mounted on the

mechanical stage for various magnet to magnet separation distances d_m. The images

were then imported into ImageJ (NIH) and h_s was calculated based on the number of

pixels per unit length. Pixel calibration was based on the measured coverslip thickness

using digital calipers.

Cell culture. Coverslips (12 mm diameter, #1.5, Warner Instruments) were cleaned in a

12 M HCl solution for 12 hours, thoroughly rinsed with DI H_2O (18.2 MΩ·cm) and stored

in 200 proof ethanol. Coverslips used for cell culturing were removed from the ethanol

and placed into tissue culture plates (Falcon 24 well plate) filled with sterile DI H_2O. The

liquid was then aspirated and filled with 0.01 mg/ml poly-L-lysine (PLL) (Sigma Aldrich)

in PBS and allowed to incubate for 12 hours at room temperature, rinsed with 2x with DI

H_2O and sterilized under UV irradiation for 20 minutes. Higher density cultures were

also achieved by plating cells onto sterilized coverslips incubated 63 nM fibronectin

(Sigma Aldrich) prepared in PBS at 2 °C overnight. Culture wells were then filled with

500 μl of cell culture media (DMEM/F12 (ThermoFisher), 20% fetal bovine serum

(LifeTechnologies), 1x penicillin-streptomycin (LifeTechnologies), 1x MEM non-essential

amino acids (LifeTechnologies) and placed in an incubator (37 °C, 5% CO_2) prior to cell

culture preparation. Primary mouse cardiomyocytes were prepared following the

methods based on the work of Sreejit *et al.*[58] and briefly described below. Neonatal

mice (C57BL/6) between P0 to P3 were decapitated and whole hearts were excised,

transferred to an ice-cold bath of dissection solution (D1), containing 2.35 mg/ml

HEPES, 8 mg/ml NaCl, 0.4 mg/ml KCl, 0.045 mg/ml $Na_2HPO_4 \cdot 7H_2O$, 1.2 mg/ml glucose,

3 mg/ml sucrose, 0.0012 mg/ml phenol red, in 18.2 MΩ·cm DI H_2O, adjusted to pH=7.3,

330 mOsm and sterile filtered, where blood was squeezed gently from the heart with

sterile forceps, then transferred to a second ice cold bath of D1 for an additional 10

minutes. Excess tissue was then removed, and the ventricles were cut into ~ 1 mm^3

size pieces. Ventricle tissue was then enzymatically dissociated in a 15 ml conical tube

using papain solution (0.15 mM $CaCl_2$, 0.5 mM EDTA, 1 mM L-cysteine, 200 units

papain (Worthington), 3 mM NaOH in 10 ml of D1) and placed on a nutating mixer at 37

°C for 30 minutes. The papain solution was then aspirated off and discarded and 2 ml of

fresh cell culture media was added. The tissue was then triturated with a fire polished

pipette (~10x), allowed to sit for 1 minute, and the supernatant single cell suspension

was collected. This process was repeated 2x. The single cell suspension was then spun

down in a centrifuge at 200G for 5 minutes at room temperature and re-suspended in

cell culture media by gentle pipetting. This technique yields ≈ $2 \cdot 10^6$ cells per neonatal

heart. Cells were then plated onto PLL or fibronectin coated coverslips at a density of ≈

125,000 cells/cm^2. Cultures were grown in a tissue culture incubator (37 °C, 5% CO_2), in

cell culture media and exchanged twice a week.

MEA measurement. Spontaneous extra-cellular field potentials were observed in

primary cardiomyocyte cultures using the MEA2100-120-system (Multi-Channel

Systems). The multi-electrode arrays (MEAs) were equipped with 120 TiN recording

electrodes with a 30 μm diameter, 100 μm pitch and ≈ 40 kΩ impedance at 1 kHz.

Lowering cells to the MEA surface. Prior to recording, the MEA was sterilized under UV

irradiation for 20 minutes. The glass ring reservoir of the MEA was filled with cell culture

media (warmed to 37 °C) and placed in a tissue culture incubator for 10 minutes (37 °C,

5% CO_2) to equilibrate. In a sterile cell culture hood, coverslips containing the

cardiomyocyte cultures were gently removed from multi-well plates using sterile forceps

and mounted onto the silicone column of the micro-positioning stage with a dab of high-

vacuum grease (Dow Corning). The cardiomyocyte culture, mounted on the micro-

positioning stage, was placed around the glass ring of the MEA to rest a fixed distance

above the recording electrodes. The resting height of the coverslip was vertically offset

using indexing spacers made of sandwiched glass coverslips (160 μm thick, #1.5,

Warner Instruments) to adjust the ≈ 240 μm dynamic range of the stage (see Figure 2

for schematic details of the mechanical stage mounted on the MEA). The stage was

lowered until signals were observed by the MEA and modulated to study spatial

dependence of the extra-cellular field potentials. After use, the stage was taken off of

the MEA, the coverslip was removed from the stage and placed back into a multi-well

plate containing culture media or discarded. The stage was then rinsed using a squirt

bottle with acetone, followed by isopropanol and DI H_2O (18.2 MΩ·cm), then sterilized

under UV irradiation for 20 minutes prior to reuse. The MEA was rinsed using a squirt

bottle with 1% (w/v) tergazyme solution in DI H_2O, followed by acetone, isopropanol and

DI H_2O rinses, then dried with a ultra-high purity nitrogen spray gun and sterilized under

UV irradiation for 20 minutes prior to reuse.

Data collection and spike detection. Voltage signals measured from MEAs were

sampled at 20 kHz using Multi Channel Experimenter (Multi-Channel Systems) and

converted to HDF5 file format. Spike detection was performed using custom software

written in Python.[59] First, data was band pass filtered (2nd order butterworth filter with

cutoff frequencies of 0.2 and 4 kHz) and spikes were detected by using a threshold to 5

times the rms-noise value. To generate spike triggered average waveforms, custom

code written in MATLAB (MathWorks) was used to extract individual voltage vs. time

waveform traces (centered about their spike time), then averaged together. Peaks were

defined by the maximum negative deflection peak greater than 5 times the rms-noise

(using the findpeak function) on unprocessed data.

Analysis of spatiotemporal signal propagation. Custom code written in MATLAB was

used to identify time-lags between all spiking electrode channels recorded by the MEA

that satisfied the spike detection criteria (mentioned previously). Time lags were

calculated by performing pairwise cross correlations (using the xcov function) between

the earliest spiking electrode (reference signal) and all other active spiking electrodes.

The spike delay times were determined by the lag-time associated with the maximum

correlation within a 10 ms time window. The spike delay times for each electrode (with

respect to the reference signal) were then used to generate a spatial map of spike

activation time across the MEA.

Cell staining and confocal microscopy imaging. Cell cultures were stained with the plasma membrane stain Wheat Germ Agglutinin-Alexa Fluor 488 (ThermoFisher), following the manufacturers protocol for cell fixation and permeabilization. Fixed cells were then mounted on glass slides using ProLong Diamond Mountant with DAPI (LifeTechnologies). Confocal z-stacks were captured with a Leica SP8 resonant scanning confocal microscope using a 63x oil immersion objective.

Acknowledgements

Author contributions

T.S. designed, built the system and carried out biological experiments. P.K.H.

contributed to the system design. M.A.H. contributed to cell culture preparation and

microscopy. T.S., P.K.H. and K.S.K. contributed to experimental discussions and wrote

the manuscript.

Additional information

Competing interests. K.S.K. serves as a consultant and has shares in ADRx, serves

as co-director of the Tau Consortium and is on the scientific advisory board of Cohen

Veterans Bioscience. The remaining authors declare that they have no competing

interests.

References

1   B. M. Maoz, A. Herland, E. A. Fitzgerald, T. Grevesse, C. Vidoudez, A. R. Pacheco, S. P. Sheehy, T. E. Park, S. Dauth, R. Mannix, N. Budnik, K. Shores, A. Cho, J. C. Nawroth, D. Segrè, B. Budnik, D. E. Ingber and K. K. Parker, *Nat. Biotechnol.*, 2018, **36**, 865–874.

2   E. W. Esch, A. Bahinski and D. Huh, *Nat. Rev. Drug Discov.*, 2015, **14**, 248–260.

3   S. N. Bhatia and D. E. Ingber, *Nat. Biotechnol.*, 2014, **32**, 760–772.

4   A. K. Capulli, K. Tian, N. Mehandru, A. Bukhta, S. F. Choudhury, M. Suchyta and K. K. Parker, *Lab Chip*, 2014, **14**, 3181–3186.

5   Y. Maury, J. Côme, R. A. Piskorowski, N. Salah-Mohellibi, V. Chevaleyre, M. Peschanski, C. Martinat and S. Nedelec, *Nat. Biotechnol.*, 2015, **33**, 89–96.

6   J. Lu, X. Zhong, H. Liu, L. Hao, C. T. L. Huang, M. A. Sherafat, J. Jones, M. Ayala, L. Li and S. C. Zhang, *Nat. Biotechnol.*, 2016, **34**, 89–94.

7   M. A. Lancaster, N. S. Corsini, S. Wolfinger, E. H. Gustafson, A. W. Phillips, T. R. Burkard, T. Otani,
        F. J. Livesey and J. A. Knoblich, *Nat. Biotechnol.*, 2017, **35**, 659–666.

8   F. Birey, J. Andersen, C. D. Makinson, S. Islam, W. Wei, N. Huber, H. C. Fan, K. R. C. Metzler, G.
        Panagiotakos, N. Thom, N. A. O'Rourke, L. M. Steinmetz, J. A. Bernstein, J. Hallmayer, J. R.
        Huguenard and S. P. Pasca, *Nature*, 2017, **545**, 54–59.

9   M. J. Birket, M. C. Ribeiro, A. O. Verkerk, D. Ward, A. R. Leitoguinho, S. C. Den Hartogh, V. V.
        Orlova, H. D. Devalla, V. Schwach, M. Bellin, R. Passier and C. L. Mummery, *Nat. Biotechnol.*,
        2015, **33**, 970–979.

10   S. I. Protze, J. Liu, U. Nussinovitch, L. Ohana, P. H. Backx, L. Gepstein and G. M. Keller, *Nat.
        Biotechnol.*, 2017, **35**, 56–68.

11   K. Ronaldson-Bouchard, S. P. Ma, K. Yeager, T. Chen, L. J. Song, D. Sirabella, K. Morikawa, D.
        Teles, M. Yazawa and G. Vunjak-Novakovic, *Nature*, 2018, **556**, 239–243.

12   K. S. Kosik, *Nature*, 2013, **503**, 31–32.

13   A. P. Alivisatos, M. Chun, G. M. Church, K. Deisseroth, J. P. Donoghue, R. J. Greenspan, P. L.
        McEuen, M. L. Roukes, T. J. Sejnowski, P. S. Weiss and R. Yuste, *Science*, 2013, **339**, 1284–1285.

14   A. P. Alivisatos, A. M. Andrews, E. S. Boyden, M. Chun, G. M. Church, K. Deisseroth, J. P.
        Donoghue, S. E. Fraser, J. Lippincott-Schwartz, L. L. Looger, S. Masmanidis, P. L. McEuen, A. V
        Nurmikko, H. Park, D. S. Peterka, C. Reid, M. L. Roukes, A. Scherer, M. Schnitzer, T. J. Sejnowski, K.
        L. Shepard, D. Tsao, G. Turrigiano, P. S. Weiss, C. Xu, R. Yuste and X. Zhuang, *ACS Nano*, 2013, **7**,
        1850–66.

15   M. E. Spira and A. Hai, *Nat. Nanotechnol.*, 2013, **8**, 83–94.

16   D. Tsai, D. Sawyer, A. Bradd, R. Yuste and K. L. Shepard, *Nat. Commun.*, 2017, **8**, 1802.

17   J. Müller, M. Ballini, P. Livi, Y. Chen, M. Radivojevic, A. Shadmani, V. Viswam, I. L. Jones, M.
        Fiscella, R. Diggelmann, A. Stettler, U. Frey, D. J. Bakkum and A. Hierlemann, *Lab Chip*, 2015, **15**,
        2767–2780.

18   M. E. J. Obien, K. Deligkaris, T. Bullmann, D. J. Bakkum and U. Frey, *Front. Neurosci.*, 2015, **9**, 423.

19   J. Abbott, T. Ye, L. Qin, M. Jorgolli, R. S. Gertner, D. Ham and H. Park, *Nat. Nanotechnol.*, 2017,
        12, 460–466.

20   B. C. Wheeler and G. J. Brewer, *Proc. IEEE*, 2010, **98**, 398–406.

21   S. Dauth, B. M. Maoz, S. P. Sheehy, M. A. Hemphill, T. Murty, M. K. Macedonia, A. M. Greer, B.
        Budnik and K. K. Parker, *J. Neurophysiol.*, 2017, **117**, 1320–1341.

22   B. J. Dworak and B. C. Wheeler, *Lab Chip*, 2009, **9**, 404–410.

23   B. M. Maoz, A. Herland, O. Y. F. Henry, W. D. Leineweber, M. Yadid, J. Doyle, R. Mannix, V. J.
        Kujala, E. A. FitzGerald, K. K. Parker and D. E. Ingber, *Lab Chip*, 2017, **17**, 2294–2302.

24   E. Moutaux, B. Charlot, A. Genoux, F. Saudou and M. Cazorla, *Lab Chip*, 2018, **18**, 3425–3435.

25   E. Ostuni, R. G. Chapman, M. N. Liang, G. Meluleni, G. Pier, D. E. Ingber and G. M. Whitesides,
        Langmuir, 2001, **17**, 6336–6343.

26   G. M. Whitesides, E. Ostuni, X. Jiang and D. E. Ingber, *Annu. Rev. Biomed. Eng.*, 2001, **3**, 335–73.

27   O. Feinerman, A. Rotem and E. Moses, *Nat. Phys.*, 2008, **4**, 967–973.

28   G. Mahmud, C. J. Campbell, K. J. M. Bishop, Y. A. Komarova, O. Chaga, S. Soh, S. Huda, K. Kandere-Grzybowska and B. A. Grzybowski, *Nat. Phys.*, 2009, **5**, 606–612.

29   D. E. Koser, A. J. Thompson, S. K. Foster, A. Dwivedy, E. K. Pillai, G. K. Sheridan, H. Svoboda, M. Viana, L. D. F. Costa, J. Guck, C. E. Holt and K. Franze, *Nat. Neurosci.*, 2016, **19**, 1592–1598.

30   A. J. S. Ribeiro, Y.-S. Ang, J.-D. Fu, R. N. Rivas, T. M. A. Mohamed, G. C. Higgs, D. Srivastava and B. L. Pruitt, *Proc. Natl. Acad. Sci.*, 2015, **112**, 12705–12710.

31   J. Moreland, S. Alexander, M. Cox, R. Sonnenfeld and P. K. Hansma, *Appl. Phys. Lett.*, 1983, **43**, 387–388.

32   J. Moreland and P. K. Hansma, *Rev. Sci. Instrum.*, 1984, **55**, 399–403.

33   H. Liu, D. Bridges, C. Randall, S. A. Solla, B. Wu, P. K. Hansma, X. Yan, K. S. Kosik and K. Bouchard, *bioRxiv*, 2017, DOI: 10.1101/204594.

34   E. Claverol-Tinture and J. Pine, *J. Neurosci. Methods*, 2002, **117**, 13–21.

35   M. D. Halbach, U. Egert, J. Hescheler and K. Banach, *Cell. Physiol. Biochem.*, 2003, **13**, 271–284.

36   M. Taketani and M. Baudry, *Advances in Network Electrophysiology*, Springer, 2006.

37   J. Dunlop, M. Bowlby, R. Peri, D. Vasilyev and R. Arias, *Nat. Rev. Drug Discov.*, 2008, **7**, 358–368.

38   A. Stett, U. Egert, E. Guenther, F. Hofmann, T. Meyer, W. Nisch and H. Haemmerle, *Anal. Bioanal. Chem.*, 2003, **377**, 486–495.

39   E. G. Navarrete, P. Liang, F. Lan, V. Sanchez-Freire, C. Simmons, T. Gong, A. Sharma, P. W. Burridge, B. Patlolla, A. S. Lee, H. Wu, R. E. Beygui, S. M. Wu, R. C. Robbins, D. M. Bers and J. C. Wu, *Circulation*, 2013, **128**, S3–S13.

40   P. L. Nunez and R. Srinivasan, *Electric Fields of the Brain: The neurophysics of EEG*, 2009.

41   C. Gold, D. A. Henze, C. Koch and G. Buzsáki, *J Neurophysiol*, 2006, **95**, 3113–3128.

42   G. Buzsáki, C. a Anastassiou and C. Koch, *Nat. Rev. Neurosci.*, 2012, **13**, 407–20.

43   M. P. Davies, R. H. An, P. Doevendans, S. Kubalak, K. R. Chien and R. S. Kass, *Circ Res*, 1996, **78**, 15–25.

44   M. S. Spach, J. F. Heidlage, P. C. Dolber and R. C. Barr, *Circ. Res.*, 2000, **86**, 302–311.

45   J. D. Jackson, *Classical Electrodynamics*, Third Edit., 1998.

46   G. Meiry, Y. Reisner, Y. Feld, S. Goldberg, M. Rosen, N. Ziv and O. Binah, *J. Cardiovasc. Electrophysiol.*, 2001, **12**, 1269–1277.

47   L. G. J. Tertoolen, S. R. Braam, B. J. van Meer, R. Passier and C. L. Mummery, *Biochem. Biophys. Res. Commun.*, 2018, **497**, 1135–1141.

48   M. Yamamoto, H. Honjo, R. Niwa and I. Kodama, *Cardiovasc. Res.*, 1998, **39**, 360–372.

49   C. Sprössler, M. Denyer, S. Britland, W. Knoll and A. Offenhäusser, *Phys. Rev. E - Stat. Physics, Plasmas, Fluids, Relat. Interdiscip. Top.*, 1999, **60**, 2171–2176.

50   J. Hescheler, M. Halbach, U. Egert, Z. J. Lu, H. Bohlen, B. K. Fleischmann and M. Reppel, *J. Electrocardiol.*, 2004, **37**, 110–116.

51   I. Kehat, A. Gepstein, A. Spira, J. Itskovitz-Eldor and L. Gepstein, *Circ. Res.*, 2002, **91**, 659–661.

52   H. Zhu, K. S. Scharnhorst, A. Z. Stieg, J. K. Gimzewski, I. Minami, N. Nakatsuji, H. Nakano and A. Nakano, *Sci. Rep.*, 2017, **7**, 1–9.

53   A. Natarajan, M. Stancescu, V. Dhir, C. Armstrong, F. Sommerhage, J. J. Hickman and P. Molnar, *Biomaterials*, 2011, **32**, 4267–4274.

54   D. J. Bakkum, U. Frey, M. Radivojevic, T. L. Russell, J. Müller, M. Fiscella, H. Takahashi and A. Hierlemann, *Nat. Commun.*, 2013, **4**, 2181.

55   D. Dumitru, *Muscle and Nerve*, 2000, **23**, 1667–1685.

56   M. A. Crackower, G. Y. Oudit, I. Kozieradzki, R. Sarao, H. Sun, T. Sasaki, E. Hirsch, A. Suzuki, T. Shioi, J. Irie-Sasaki, R. Sah, H. Y. M. Cheng, V. O. Rybin, G. Lembo, L. Fratta, A. J. Oliveira-dos-Santos, J. L. Benovic, C. R. Kahn, S. Izumo, S. F. Steinberg, M. P. Wymann, P. H. Backx and J. M. Penninger, *Cell*, 2002, **110**, 737–749.

57   L. Formigli, F. Francini, S. Nistri, M. Margheri, G. Luciani, F. Naro, J. D. Silvertown, S. Z. Orlandini, E. Meacci and D. Bani, *J. Mol. Cell. Cardiol.*, 2009, **47**, 335–345.

58   P. Sreejit, S. Kumar and R. S. Verma, *Vitr. Cell. Dev. Biol. - Anim.*, 2008, **44**, 45–50.

59   D. C. Bridges, K. R. Tovar, B. Wu, P. K. Hansma and K. S. Kosik, *PLoS One*, 2018, **13**, e0192477.

A single set of electrical sensors can probe the activity of electrogenic cells grown on disposable coverslips without degrading its performance.